

Numerical investigations of active control of boundary-layer instabilities

Christoph Gmelin, Ulrich Rist, and Siegfried Wagner

IAG, Universität Stuttgart, Pfaffenwaldring 21, 70550 Stuttgart, Germany

rist@iag.uni-stuttgart.de,

WWW home page: <http://www.iag.uni-stuttgart.de>

Summary

Controlling laminar-turbulent transition in boundary layers is an important topic of future aerodynamics. With the aid of Direct Numerical Simulation (DNS) and Linear Stability Theory (LST) we examine different active approaches in various flow scenarios. The superposition of disturbances with opposite phase to the initial waves in the boundary layer leads to a significant attenuation only in linear and weakly nonlinear scenarios. In stages close to transition where strong nonlinearity has taken place we were able to develop a method which is better suited. The direct feedback of instantaneous flow data obtained at the wall (wall shear stress or spanwise vorticity) leads to better damping capabilities of nonlinear disturbances. We can show that the main mechanism of this concept lies in the change of the sign of the Reynolds stress of the participating modes. In addition, existing resonances are disrupted due to the modified phase speed of the controlled modes.

1 Introduction

In the past, mainly passive methods such as smooth surfaces or advantageous pressure distributions have been used to reduce aerodynamic drag of wings, shifting the boundary layer transition downstream. Unfortunately, beyond a certain Reynolds number these approaches don't work in a satisfactory manner. In this case, approaches which actively damp disturbances in boundary layers offer new promising possibilities.

The most popular approach controlling transition is the superposition of disturbances with opposite phase to the existing waves. First attempts have been published by Milling [1], Liepmann et al. [2, 3] and Kozlov et al. [4]. Until now, this strategy has been realized many more times both experimentally [5] and numerically [6]. For disturbances with small (linear) amplitude a reduction in amplitude of up to 90% is achievable even in experiments. In contrast to their excellent performance in early transition stages these approaches don't work in a satisfactory manner in cases where high amplitudes occur due to nonlinear effects. Moreover, the generation of control waves with

large amplitude which are necessary to cancel the initial wave with the aid of a suction/blowing slot sometimes causes very high velocities in the vicinity of these actuators, an effect which favours nonlinearities furthermore. These arguments make clear that there is a need for a smooth, robust control algorithm which is almost independent of the amplitude of the initial disturbance.

One way to actively damp even nonlinear disturbances is the application of concepts which use instantaneous flow data obtainable at the wall to drive plain actuators, like wall shear stress or spanwise vorticity. Avoiding long propagation distances between sensor and actuator this procedure (called **ω_z -control**) results in a very effective damping even in nonlinear cases. Additionally, the influenced modes are attenuated in a very ‘soft’ way without the danger of producing further instabilities due to large actuator- (blowing and suction-) amplitudes.

2 Numerical Method

All simulations were performed in a rectangular integration domain with the spatial DNS-code developed by Konzelmann, Rist and Kloker [7–9].

The flow is split into a steady 2D-part (Blasius base flow) and an unsteady 3D-part. The x -(streamwise) and y -(wall-normal) directions are discretised with finite differences of fourth-order accuracy and in the spanwise direction z a spectral Fourier representation is applied. Time integration is performed by the classical fourth-order Runge-Kutta scheme. The utilised variables are normalised with $\tilde{U}_\infty = 30 \frac{m}{s}$, $\tilde{\nu} = 1.5 \cdot 10^{-5} \frac{m^2}{s^2}$ and $\tilde{L} = 0.05m$.

3 Base flow

Two different base flows, both Blasius boundary-layers have been examined. Base flow A, used for the investigation of linear scenarios and the K-breakdown (see below) features a Reynolds number based on the displacement thickness of $Re_{\delta_1} = 500$ at the inflow boundary and of $Re_{\delta_1} = 1340$ at the outflow boundary. The other one, base flow B, is needed to perform all simulations concerning point-source and white-noise excitation. Its Reynolds number at the inflow is $Re_{\delta_1} = 1000$ and $Re_{\delta_1} = 2018$ at the outflow. Its maximum amplification rate remains quite smaller than that of base flow A but its integral amplification for some frequencies turns out to be much larger.

4 Undisturbed scenarios

4.1 K-breakdown

The most important test case for all control approaches is a typical K-breakdown scenario as shown in Fig. 1, where transition due to fundamental

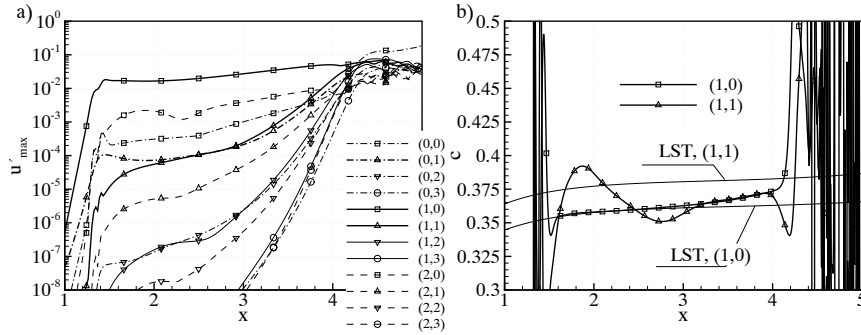


Figure 1 K-breakdown: Transition due to fundamental resonance between the modes (1,0) and (1,1) (thick lines). a) u' -amplitudes, b) phase speed c of the resonant modes

resonance between discrete modes (with the same frequency) occurs. Here, the modes (1,0) and (0,1) (the first index denotes multiples of the fundamental frequency $\beta=10$, the second multiples of the basic spanwise wave number $\gamma = 20$) are forced. The (fundamental) mode (1,0) is a 2D-mode excited with large, nonlinear amplitude, whereas the mode (0,1) is a steady mode with small amplitude. The modes (1, \pm 1) are instantly generated as direct higher-harmonics of the two initially generated modes. At $x \approx 2$ a rapid increase in amplitude of the modes (0,1) and (1, \pm 1) can be observed. Simultaneously, the phase of the resonant modes (1, \pm 1) is synchronised to that of the fundamental one, i.e. their phase speeds become equal (Fig. 1 b)). These observations strongly indicate the presence of fundamental resonance between the large 2D- and the smaller 3D-mode. When the amplitude of the amplified 3D-waves has reached the level of the fundamental mode the amplitudes of all modes saturate on a high level and the transition to turbulence takes place. Together with the increase of the 3D-amplitude the evolution of transitional structures can be observed. Figure 14 a) shows a typical aligned pattern of Λ -vortices in accordance with the detected resonance type.

4.2 Point source driven by white noise

Besides the extensively investigated K-breakdown a second transition scenario was investigated. The simulation of a white noise scenario in base flow B was stimulated by the wish of having a more ‘natural’ environment to show the effects of active control. Following Gaster & Shaikh (e.g. [10]) a point source with zero net mass flux (Fig. 2) is activated by a fixed time sequence.

This sequence (Fig. 3) has a length of 20 periods of the most unstable frequency ($\beta = 6$) and consists of a broad range of frequencies from $\beta = 0.3$

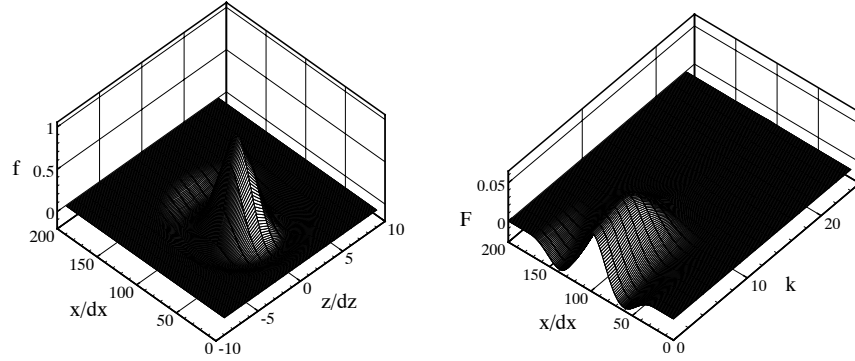


Figure 2 Disturbance function of the point source in physical space (left) and in Fourier space (right; $\gamma_0 = 3$, $\gamma = k \cdot \gamma_0$).

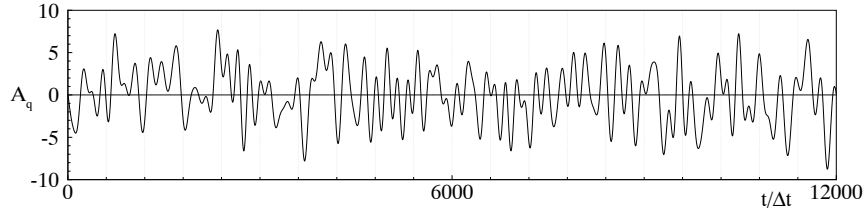


Figure 3 Time sequence for the excitation of the point source. The sequence is repeated every 20 periods (of the most amplified frequency $\beta = 6$), every period is divided into 600 time steps.

to $\beta = 24$, all spectral portions having the same amplitude. The excitation results in a sequence of three-dimensional wave packets generating various nonlinear interactions further downstream (Fig. 5).

Analysing this scenario with ‘traditional’ Fourier techniques doesn’t lead to a satisfactory result, because of the distributing nature of the Fourier transform (single events can’t be located in time). Therefore, we analyse the time signals of the spanwise wall-vorticity with aid of the continuous wavelet transform using a Morlet-mother-wavelet [11] at a fixed x -position. The resulting wavelet-spectrum (Fig. 4) is similar to a Fourier-spectrum, but time dependent. It shows, besides the linear portion of the time signal (maxima around $\beta \approx 7$ and $\gamma = 0$) additional local maxima at a spanwise wave number of $\gamma \approx 15$ near the subharmonic frequency of the linear modes. Due to the wavepacket-like complex mother-wavelet it is possible to calculate amplitudes, phases and even phase speeds of the modes subject to frequency and

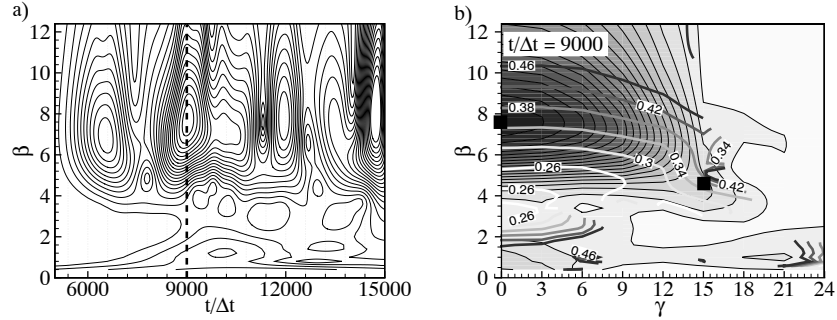


Figure 4 Wavelet transform of the spanwise vorticity at the wall (Morlet mother-wavelet with $\omega_0 = 3$), $x = 7.25$. a): Amplitudes for $\gamma = 0$, b): Amplitudes and phase speed versus frequency and spanwise wave number. Resonant modes are marked by a black square.

time. Analysing the matching phase-speeds of the modal groups which are involved, we come to the conclusion, that the dominating resonance mechanism neither is fundamental nor subharmonic but ‘detuned’ with three participating modal groups. For the one wavepacket observed in Fig. 4 b) we find a fundamental 2D mode at $\beta \approx 7.6$, $\gamma = 0$ and two resonant 3D modes at $\gamma \approx 15$, $\beta \approx 4.6$ and $\beta \approx 3.0$. Although not visible in Fig. 4 b) the second resonant mode with $\beta \approx 3.0$ must exist to complete the resonant wave triad. A look at the dotted lines of Fig. 15 (further discussion of this figure in the active control section) shows almost the same strong amplification rate for both resonant modes which is a further clue for that kind of detuned resonance. Compared to the modal evolution of the K-breakdown scenario, where discrete modes are at work, one must consider that modal groups interact with each other in the present case.

5 Active Control

5.1 Superposition of anti-phase disturbances

The first control method we investigated was the well tested (experimental [13] and numerical [14]) wave superposition approach. This ‘classical’ approach is basically limited to linear 2D and 3D disturbances because superposition of several modes without the generation of new modal products is only possible when the amplitude of the initial disturbance is small. For such a case, single modes can be attenuated by adding an identical but anti-phase wave. Theoretically, with proper amplitude and phase of the control wave complete cancellation of the initial wave is possible [15] but due to inevitable deviations from the ideal case in practice this goal is never reached. The

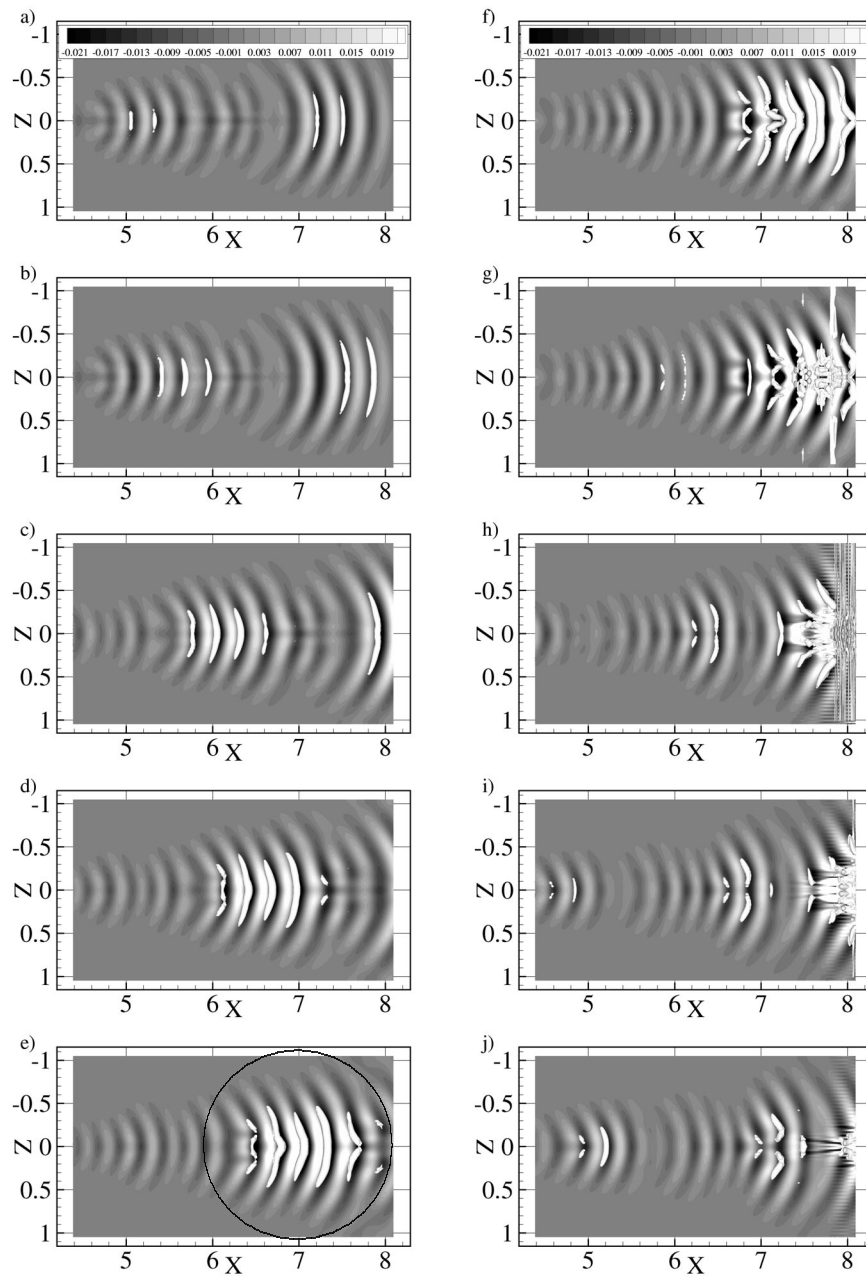


Figure 5 White noise excitation. Spanwise vorticity at the wall plus vortex structures, visualized with aid of the λ_2 -method [12]. The time step between two pictures corresponds to one period of $\beta = 6$.

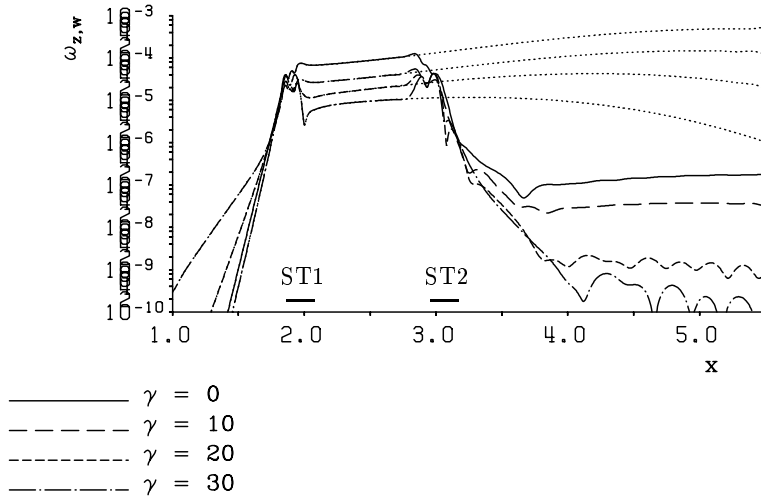


Figure 6 Active control of linear waves with different spanwise wave numbers ($\beta = 10$, base flow A). Fourier amplitudes of the spanwise vorticity at the wall $\omega_{z,w}$. Dotted lines: uncontrolled case; ST1 and ST2 = disturbance and control strip, respectively.

simulation of the linear case (Fig. 6) nevertheless shows, that for both 2D- and 3D TS-waves a reduction of the initial amplitude of approximately three orders of magnitude is achievable.

The extension of this concept towards arbitrary linear disturbances leads to the use of temporal FIR-filters to produce the necessary counter-disturbance similar to those already used in experimental investigations [16]. The (physical) filter corresponds to a complex transfer function between sensor- and actuator-signal in Fourier space. It has to be trained for each flow condition to suit the local flow conditions or has to be adapted continuously. To avoid time-consuming calculations, in our case the filter was trained once to obtain the filter coefficients for subsequent runs [15].

Active control via FIR-filters at different streamwise positions is now compared in Fig. 7 for the K-breakdown scenario already used above. Here, control is applied only to the fundamental 2D-mode which is evolving in an almost linear way. Depending on the position of the control strip (ST2), the results nicely show how the efficiency of the wave-superposition principle diminishes with downstream distance due to non-linear effects. Only because of its ‘quasi-linear’ behaviour (with respect to phase speed or amplification) we are initially able to control this mode. The resonant 3D-modes are not controllable via the same mechanism, because they are completely coupled to the fundamental 2D-mode and do not show any linear (i.e. independent)

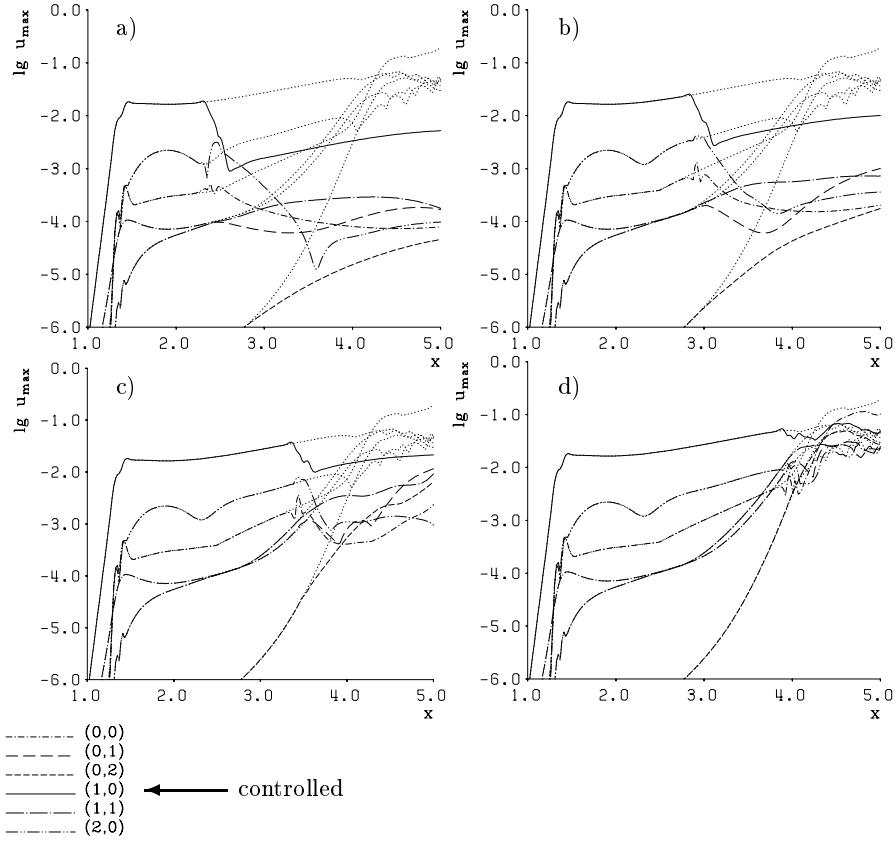


Figure 7 K-Breakdown: Active control of the fundamental mode (1,0) via wave superposition at different downstream stations. a) $x = 2.41$, b) $x = 2.94$, c) $x = 3.46$, d) $x = 3.98$. Dotted lines: uncontrolled case for reference.

behaviour. However, as soon as the primary 2D disturbance is damped the phase-coupling of the modes (1,0) and (1,1) is broken up and the resonant modes don't possess the same phase speed any more [17], which is necessary for an efficient energy transfer. Thus, a further amplification of the 3D-modes is prevented (compared to the dotted reference lines). The remaining steady 3D disturbance modes (0,k) are very difficult to control. They exhibit some kind of transient growth for large x (especially visible in Fig. 7 b) and c)).

5.2 ω_z -Control

Another way to actively damp disturbances in boundary layers is the feedback of instantaneous signals, e.g. of the spanwise vorticity fluctuations (ω_z) measured at the wall. These signals are prescribed as a v -boundary condition at the wall after multiplication by a complex amplitude A (whose imaginary part causes the phase shift Φ shown in Fig. 8).

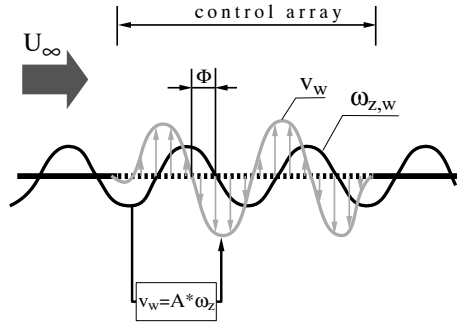


Figure 8 ω_z control

First, results of DNS are analysed in order to show how the method works in the linear case. For a small-amplitude 2D Tollmien-Schlichting (TS-) wave three simulation results are presented in Fig. 9: one for the reference case without control, one with control applied, and the third shows the results obtained for the control signal alone. Throughout the control strip a gradual amplitude reduction can be observed for the controlled case in Fig. 9 a).

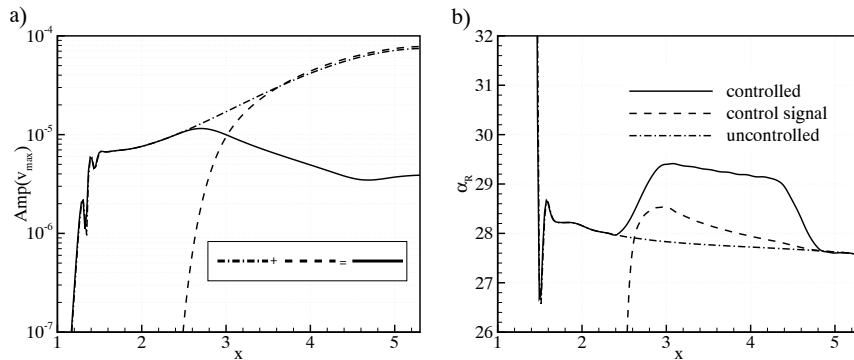


Figure 9 Comparison of v -amplitudes (a) and wave numbers (b) with and without ω_z -control. Additionally one can observe the control signal ($|A| = 7.5 \cdot 10^{-5}$, no phase difference between ω_z and v_w , the control array reaches from $x = 2.4$ to 4.8). Base flow A. Every curve represents a single simulation.

In wave-superposition control, where an anti-phase disturbance of the same frequency and wave number is superimposed on the initial perturbation, frequency and wave number of both disturbances would be the same.

Figure 9 b) clearly indicates that this is not the case using the ω_z -control, because the wave number α_R and therefore the phase velocity c_{ph} of the controlled wave differs from the uncontrolled case. These results show, that this approach is completely different to the wave-superposition principle.

LST Results To get an overview of the damping capabilities of the present concept and to optimise the parameters for further simulations, investigations using linear stability theory (LST) have been performed. Therefore, the boundary conditions at the wall for the Orr-Sommerfeld (and Squire) equation had to be changed. The amplification-factor between v_w and $\omega_{z,w}$ is expressed as a complex number $A = |A| \cdot e^{i\Phi}$ allowing a variable phase Φ between sensor- and actuator signal.

A strong damping effect and a significant reduction of the unstable area in the stability diagram (Fig. 10) is already caused by very small amplitudes $|A|$. Results of a detailed investigation of the influence on the most unstable eigenvalues are presented in Fig. 11 for an amplitude of $2 \cdot 10^{-5}$ and a variation of the phase angle Φ between v_w and $\omega_{z,w}$. The computation of the eigenvalues shows, that there is a strong dependence on the phase angle. One can find the largest possible damping for all modes in the region of $\Phi \approx \frac{\pi}{4} \dots \frac{\pi}{2}$. Therefore, to achieve the desired damping effect it is most important to use an according phase angle between v_w and $\omega_{z,w}$.

Energy Properties A deeper insight into the acting mechanisms can be obtained by looking at the spatial linear 2D energy balance equation

$$\begin{aligned} \underbrace{\frac{1}{2} \frac{\partial}{\partial x} \int_0^\infty u_B (\overline{u'^2} + \overline{v'^2} + \overline{w'^2}) dy}_{\mathbf{E}} &= - \underbrace{\int_0^\infty \overline{u'v'} \frac{\partial u_B}{\partial y} dy}_{\mathbf{R}} \\ &- \underbrace{\frac{1}{Re} \int_0^\infty \overline{\omega_{ges}^2} dy}_{\mathbf{D}} - \frac{\partial}{\partial x} \int_0^\infty \overline{u'p'} dy + \overline{v'_w p'_w} - \frac{\partial}{\partial z} \int_0^\infty \overline{w'p'} dy \\ &+ \frac{1}{Re} \left(\frac{\partial}{\partial x} \int_0^\infty \overline{w'\omega'_y - v'\omega'_z} dy + \frac{\partial}{\partial z} \int_0^\infty \overline{v'\omega'_x - u'\omega'_y} dy \right). \quad (1) \end{aligned}$$

This equation is derived from the 2D Navier-Stokes equations with the aid of a parallel-flow assumption and a wave approach for the disturbances [18] (overlines denote an average over one period of time). The spatial rate of increase of fluctuation energy flux (E) can be split into the energy production (R), the dissipation (D), a pressure term and a small negligible rest (eqn. 1). Figure 12 compares the most important energy-properties for the case of an amplified TS-wave with and without active control. The application of ω_z -control at $x > 2.4$ changes the sign of the energy flux together with the curves for production and pressure term. Clearly, the energy production term

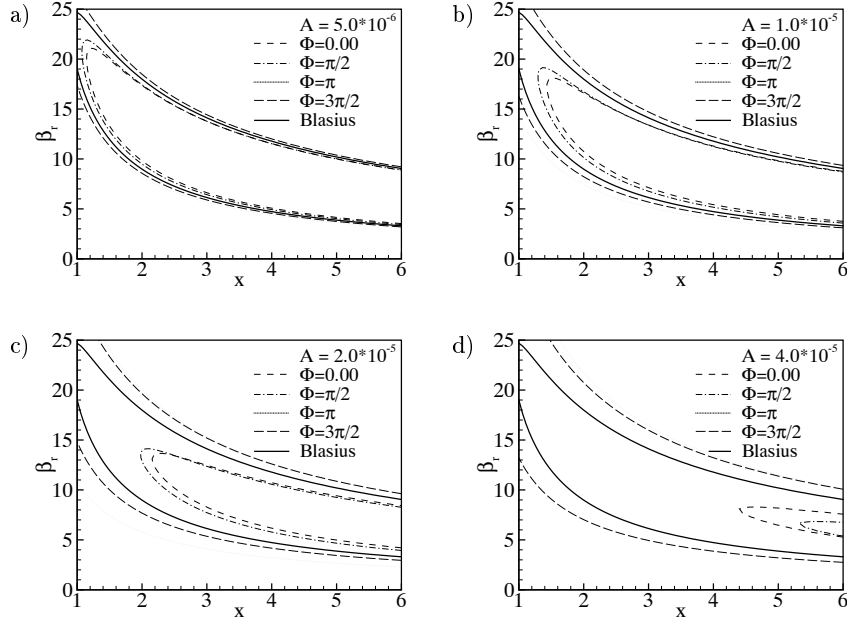


Figure 10 Neutral Curves ($\alpha_i = 0$) of 2D-TS-modes in the Blasius boundary layer A according to LST with active control applied. (a): $|A| = 5 \cdot 10^{-6}$, (b): $|A| = 1 \cdot 10^{-5}$, (c): $|A| = 2 \cdot 10^{-5}$, (d): $|A| = 4 \cdot 10^{-5}$.

R dominates the complete energy balance. Its sign, respectively the sign of the Reynolds stress $\overline{u'v'}$ (see eqn. 1), determines the attenuation or growth of the regarded disturbance ($\overline{u'v'} > 0 \Rightarrow R < 0 \Rightarrow E < 0 \Rightarrow$ reduction of amplitude and vice versa). The change of sign of the Reynolds stress $\overline{u'v'}$ when control is applied is not caused by different u' or v' amplitudes but by its strong sensitivity to the phase difference $\Delta\theta = |\theta(u') - \theta(v')|$ around $\Delta\theta(y) = \frac{\pi}{2}$ which is altered by the non-zero v_w [19].

DNS results As a test case for the effect of the ω_z -approach on disturbances with large amplitude the well-known K-breakdown scenario from Fig. 1 is used again. Applying ω_z -control to this scenario two main control effects can be distinguished: direct damping of nonlinear disturbances and the affection of the resonant behaviour due to the influence of the control on the phase speed of the controlled modes [17]. From Fig. 11 it is obvious that the optimal phase shift between ω_z and v is more or less independent of the frequency. Thus, controlling with a fixed time delay between sensor and actuator signal yields to a different, non optimal control phase for some frequencies. To obtain the desired phase for every occurring frequency resp. wave number a spatial

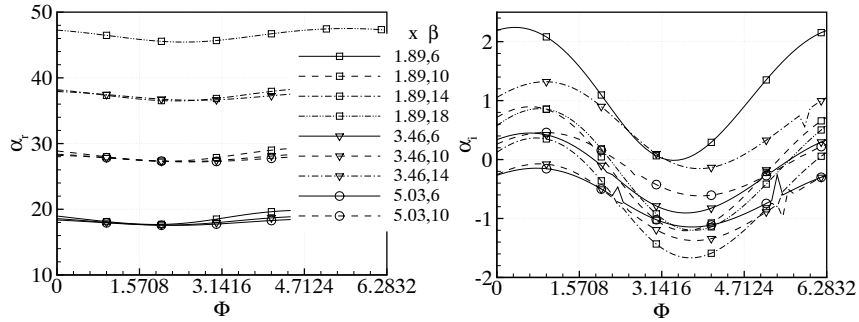


Figure 11 Dependence of wave number and amplification rate on the phase between v_w and $\omega_{z,w}$ according to LST. $|A| = 2 \cdot 10^{-5}$, spanwise wavenumber $\gamma = 0$.

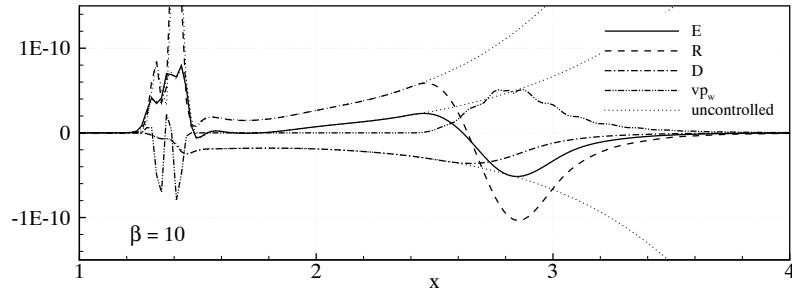


Figure 12 Downstream development of integral energy quantities. $\beta = 10$, controlled at $x > 2.4$ ($|A| = 0.0001$, $\Phi = \pi/2$). Dotted lines: uncontrolled case.

FIR-Filter is applied to the input data to treat every wave number in the same way. In terms of Fourier space the (transformed) sensor signal is multiplied by a complex transfer function to obtain the actuator output. Thus, it is possible to filter the input data as a function of their spatial wavenumber and to choose the optimal phase relation for every mode. An additional desired effect is the prevention of instabilities, which might be introduced unintentionally by the actuator response to the flow field.

Investigations applying ω_z -control in combination with a spatial filter in late nonlinear stages of the K-breakdown to both 2D and 3D modes indicate that an amplitude reduction of more than one order of magnitude is possible. Figure 13 shows a simulation with control of the 2D ($\dots, 0$) and 3D ($\dots, 1$) modes where the control array extends from $x = 3.5$ to $x = 5.0$. The control amplitude is turned on via a spatial ramp function which is also shown. With such

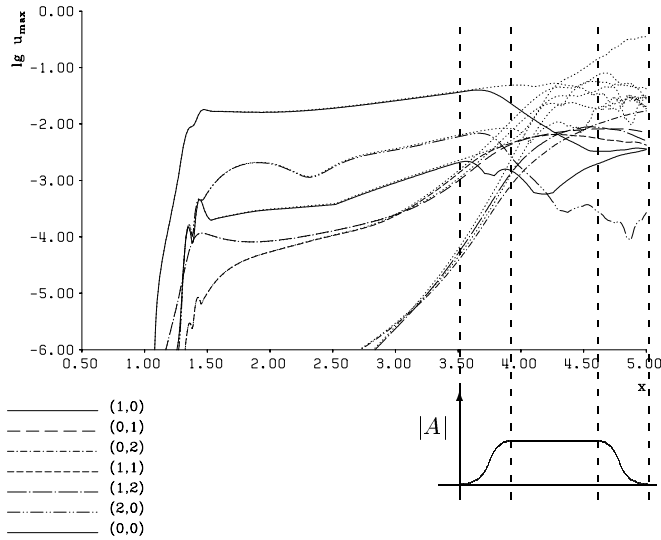


Figure 13 K-Breakdown, u_{max} -amplitudes. Active control of the 2D- and 3D-modes by application of ω_z -control in combination with a spatial FIR-filter ($|A| = 1.5 \cdot 10^{-4}$). Dotted lines: uncontrolled scenario. Small picture: control amplitude $|A|$ vs. x .

an arrangement it is possible to prevent the occurrence of transitional flow structures such as Λ -vortices or high shear layers when active control is applied only two wavelengths prior to their first appearance in the uncontrolled case (Fig. 14).

As with other unsteady control strategies ω_z -control is not well suited for steady modes. Only by damping the fluctuating parts of the disturbance the nonlinear generation of these modes can be inhibited. Compared to the K-breakdown scenario controlled via wave superposition, it is possible to successfully damp disturbances in later stages. Here we can control 2D- and 3D-modes because the ω_z -approach does not require linear modal properties of these disturbances due to its mechanisms and the loss of a spatial control path between sensor and actuator.

To confirm the results obtained for the K-breakdown case and to test our approach in a more ‘natural’ environment, we investigated the behaviour of the disturbances emanating from a point source driven by white noise (section 4.2) under the influence of our active control scheme. These more 3D-dominated disturbances can not be damped by just controlling the 2D-part of the signal. Therefore, it is necessary to use the spatial filter technique for every spanwise wave number. It turns out, that the wave-like part of the disturbances can be treated very efficiently by the ω_z -algorithm (Fig. 15), even in very late stages. Unfortunately, interaction of the damped modes

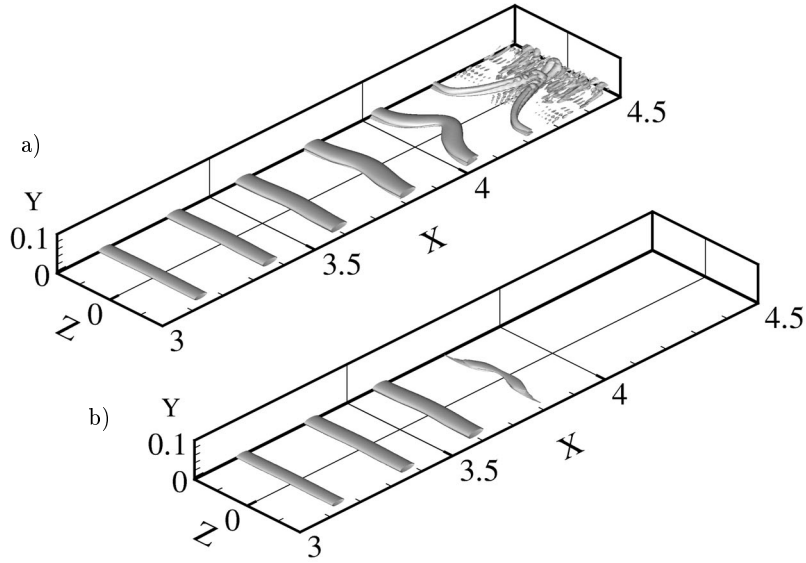


Figure 14 Vortex structures visualised with aid of the λ_2 -method [12]. a): uncontrolled case, b): controlled case. Same simulation as Fig. 13.

with the low-wavenumber part of the signal (comparable to the stationary modes seen in the K-breakdown) leads to a new growth of the disturbances near the outflow boundary ($x \gtrsim 8$).

6 Conclusions

To actively damp disturbances in a transitional boundary layer and to delay laminar-turbulent transition we used two different approaches. The first method, the superposition of anti-phase disturbances works very well as long as disturbances are small (i. e. linear superposition of waves of the same frequency is possible). Therefore, in nonlinear scenarios such a kind of control has to be applied in a very early stage of transition to work satisfactorily.

Another way of effective damping of transitional disturbances is the direct feedback of the spanwise vorticity at the wall into the flow as wall-normal velocity (ω_z -control). This method doesn't lead to an immediate fast decrease in amplitude of the controlled waves like the wave-superposition principle but to a more continuous attenuation of the controlled disturbance. On the other hand, this feature avoids excessively large suction and blowing amplitudes within the control strip. In contrast to the wave superposition, ω_z -control can be successfully applied even in later stages of transition when nonlinear interactions are already present. The range of application ends when large, vortex-like structures of the transition process are present in the boundary

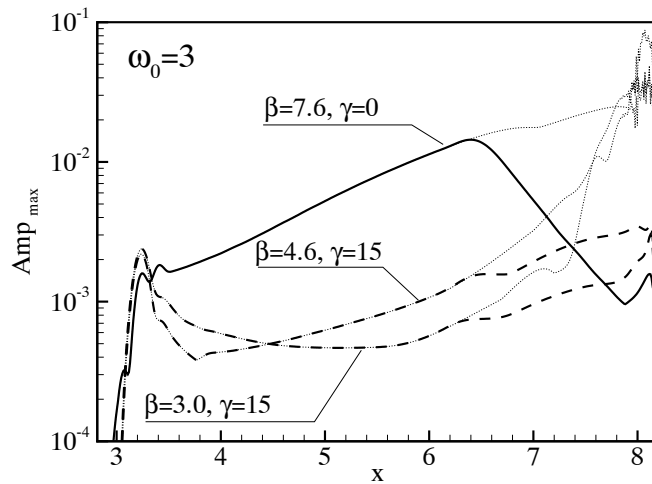


Figure 15 Downstream evolution of the maximum wavelet amplitude for several frequencies and wave numbers (especially the marked modes of Fig. 4). Active control applied for $x > 6.4$.

layer. The ω_z -approach shows remarkable improvements compared to ‘classical’ approaches but even for the most efficient approach a relaminarization of turbulent or nearly turbulent flows seems to be out of scope.

7 Acknowledgements

Performing the present investigations was only possible due to financial support by DFG within Project RI 680/8 and computer time provided by the high-performance computer center (HLRS). This support is gratefully acknowledged.

References

- [1] Milling, R.W.: Tollmien-Schlichting wave cancelation. *Phys. Fluids* **24** (1981) 979–981.
- [2] Liepmann, H.W., Brown, G.L., Nosenchuck, D.M.: Control of laminar-instability waves using a new technique. *J. Fluid Mech.* **118** (1982) 187–200.
- [3] Liepmann, H.W., Nosenchuck, D.M.: Active control of laminar-turbulent transition. *J. Fluid Mech.* **118** (1982) 201–204.

- [4] Kozlov, V.V., Levchenko, V.Y.: Laminar-turbulent transition control by localized disturbances. In Liepmann, H.W., Narasimha, R., eds.: *Turbulence Management and Relaminarisation*, IUTAM-Symposium, Bangalore, India, 1987, Springer Verlag, Berlin, Heidelberg (1987) 249–269.
- [5] Baumann, M., Nitsche, W.: Investigations of active control of Tollmien-Schlichting waves on a wing. In Henkes, R., van Ingen, J., eds.: *Transitional Boundary Layers in Aeronautics*. Volume 46. KNAW, Amsterdam, North Holland (1996) 89–98.
- [6] Laurien, E., Kleiser, L.: Numerical simulation of boundary-layer transition and transition control. *J. Fluid Mech.* **199** (1989) 403–440.
- [7] Kloker, M.: *Direkte Numerische Simulation des laminar-turbulenten Strömungsumschlages in einer stark verzögerten Grenzschicht*. Dissertation, Universität Stuttgart (1993).
- [8] Konzelmann, U.: *Numerische Untersuchungen zur räumlichen Entwicklung dreidimensionaler Wellenpakete in einer Plattengrenzschicht*. Dissertation, Universität Stuttgart (1990).
- [9] Rist, U., Fasel, H.: Direct numerical simulation of controlled transition in a flat-plate boundary layer. *J. Fluid Mech.* **298** (1995) 211–248.
- [10] Shaikh, F.N.: Investigation of transition to turbulence using white-noise excitation and local analysis techniques. *J. Fluid Mech.* **348** (1997), 29–83.
- [11] Torrence, C., Compo, G.P.: *A practical guide to wavelet analysis*. Bull. Amer. Met. Soc. (1997).
- [12] Jeong, J., Hussain, F.: On the identification of a vortex. *J. Fluid Mech.* **285** (1995) 69–94.
- [13] Baumann, M.: *Aktive Dämpfung von Tollmien-Schlichting-Wellen in einer Flügelgrenzschicht*. Dissertation, Technische Universität Berlin (1999).
- [14] Kleiser, L., Laurien, E.: Numerical simulation of boundary-layer transition and transition control. *J. Fluid Mech.* **199** (1989) 403–440.
- [15] Gmelin, C., Rist, U., Wagner, S.: Investigations of active control of wave packets and comparable disturbances in a Blasius boundary layer by DNS. In W. Nitsche, Heinemann, H.J., Hilbig, R., eds.: *Notes on Numerical Fluid Mechanics*. Volume 72. Vieweg-Verlag, Braunschweig (1998) 194–201.
- [16] Baumann, M., Sturzebecher, D., Nitsche, W.: On active control of boundary layer instabilities on a wing. In W. Nitsche, Heinemann, H.J., R. Hilbig, eds.: *Notes on Numerical Fluid Mechanics II*. Volume 72. Vieweg-Verlag, Braunschweig (1998) 22–29.
- [17] Gmelin, C., Rist, U., Wagner, S.: DNS of active control of disturbances in a blasius boundary layer. In Fasel, H., Saric, W., eds.: *Laminar-Turbulent Transition*, IUTAM-Symposium, Sedona, AZ, USA, 1999, Springer Verlag, Berlin Heidelberg (2001), 149–154.
- [18] Hama, F.R., Williams, D.R., Fasel, H.: Flow field and energy balance according to the spatial linear stability theory of the Blasius boundary layer. In: In Eppler, R., Fasel, H., eds.: *Laminar-Turbulent Transition*, IUTAM Symposium Stuttgart/Germany, 1979, Springer-Verlag (1980) 73–85.
- [19] Gmelin, C., Rist, U.: Active control of laminar-turbulent transition using instantaneous vorticity signals at the wall. *Phys. Fluids* **13** (2/2000) 513–519.